Identifying Potential Sub-Synchronous Oscillations Using Impedance Scan Approach

Preprint

Shahil Shah,[1] Jingwei Lu,[2] and Nilesh Modi[2]

1 National Renewable Energy Laboratory
2 Australian Energy Market Operator

Presented at the CIGRE Paris Session 2024
Paris, France
August 25–30, 2024

NREL is a national laboratory of the U.S. Department of Energy
Office of Energy Efficiency & Renewable Energy
Operated by the Alliance for Sustainable Energy, LLC

This report is available at no cost from the National Renewable Energy Laboratory (NREL) at www.nrel.gov/publications.

Contract No. DE-AC36-08GO28308

Conference Paper
NREL/CP-5D00-88448
August 2024

Identifying Potential Sub-Synchronous Oscillations Using Impedance Scan Approach

Preprint

Shahil Shah,[1] Jingwei Lu,[2] and Nilesh Modi[2]

1 National Renewable Energy Laboratory
2 Australian Energy Market Operator

Suggested Citation
Shah, Shahil, Jingwei Lu, and Nilesh Modi. 2024. *Identifying Potential Sub-Synchronous Oscillations Using Impedance Scan Approach: Preprint*. Golden, CO: National Renewable Energy Laboratory. NREL/CP-5D00-88448. https://www.nrel.gov/docs/fy24osti/88448.pdf.

NREL is a national laboratory of the U.S. Department of Energy
Office of Energy Efficiency & Renewable Energy
Operated by the Alliance for Sustainable Energy, LLC

This report is available at no cost from the National Renewable Energy Laboratory (NREL) at www.nrel.gov/publications.

Contract No. DE-AC36-08GO28308

Conference Paper
NREL/CP-5D00-88448
August 2024

National Renewable Energy Laboratory
15013 Denver West Parkway
Golden, CO 80401
303-275-3000 • www.nrel.gov

NOTICE

This work was authored in part by the National Renewable Energy Laboratory, operated by Alliance for Sustainable Energy, LLC, for the U.S. Department of Energy (DOE) under Contract No. DE-AC36-08GO28308. Funding provided by U.S. Department of Energy Office of Energy Efficiency and Renewable Energy Wind Energy Technologies Office. The views expressed herein do not necessarily represent the views of the DOE or the U.S. Government.

Cover Photos by Dennis Schroeder: (clockwise, left to right) NREL 51934, NREL 45897, NREL 42160, NREL 45891, NREL 48097, NREL 46526.

Identifying Potential Sub-synchronous Oscillations Using Impedance Scan Approach

Shahil SHAH
National Renewable Energy Laboratory
United States
shahil.shah@nrel.gov

Jingwei LU, Nilesh MODI*
Australian Energy Market Operator
Australia
jingwei.lu@aemo.com.au
nilesh.modi@aemo.com.au

SUMMARY

The widespread integration of inverter-based resources (IBRs) is changing power system dynamics. Many of these IBRs are deployed in remote parts of the network and in close proximity to each other. System operators globally are experiencing sub-synchronous oscillations in the grid, often in regions where a cluster of IBRs is connected. In Australia, sub-synchronous oscillations have been observed in an area which has a large penetration of IBRs. The frequency of oscillations has been between 8 Hz and 20 Hz with varying magnitude and duration. When a large part of the network is experiencing oscillations, it is important to understand their root cause. Field measurements capturing oscillations at various nodes in the system cannot answer questions such as whether any specific IBR or a group of IBRs are responsible for the oscillations, or which IBRs are positively or negatively contributing to the oscillations. Time-domain simulations might provide insights on whether control mode changes or curtailment of certain IBRs can mitigate the observed oscillations, but do not always reveal the root cause of the oscillations without extensive sensitivity analysis being undertaken. The identification of the root cause not only allows the system operator to eliminate the source of oscillations operationally, but also provides an opportunity to work with relevant generator owners to explore long-term solutions. Impedance-based frequency scans of IBRs and the network at their points of connection can provide useful insights to answer these questions.

This paper presents an impedance scan study on the power system in Australia, in which 17-20 Hz intermittent sub-synchronous oscillations have been observed. Through the impedance scan of each of the IBRs, both individually and collectively, potential resonance modes have been identified. The impedance scans were carried out using electromagnetic transient (EMT) simulation models of the network. The network comprises site-specific, black-boxed models of IBRs supplied by the generators. The impedance scan approach was divided into three major steps: (1) identification of IBRs where impedance analysis needed to be performed based on the magnitude of oscillations observed at their points of interconnection (POIs); (2) undertaking impedance scans at selected IBRs in a single-machine infinite-bus (SMIB) configuration to identify internal resonance modes of the selected IBRs and to evaluate if any of these modes became unstable under certain grid conditions; (3) undertaking impedance scans at IBRs while they were connected to the wider network model to obtain the impedance response of both the IBR and the grid to evaluate control interactions among IBRs.

The impedance scan study found that a few IBRs have a poorly damped resonance mode at around 17 Hz, which becomes unstable under a certain operating condition. Another interesting finding was that certain IBRs increase the effective grid impedance seen by another IBR in close proximity for a particular operating condition. Under this operating condition, the resulting sub-synchronous oscillation mode is more pronounced due to a combination of control interactions among IBRs through the transmission network under study and a resonance mode inside the IBRs.

KEYWORDS

oscillations, control interactions, stability, IBRs, grid strength, EMT simulation, impedance analysis.

1. Background

The Australian National Electricity Market (NEM) power system has been going through a significant transition in the past few years, from a centralized, fossil-fuel based power system, towards a power system with high penetration of inverter-based resources (IBRs). According to the Australian Energy Market Operator (AEMO)'s Quarterly Energy Dynamics report [1], by Q3 2023, peak instantaneous IBR penetration reached 70% for the NEM power system. Considering the energy that was offered by IBRs but could not be dispatched due to the market pricing mechanism, potential NEM-wide IBR penetration reached 98% by Q3 2023, highlighting a significant growth potential for future IBR penetration.

Many IBRs in the NEM power system are connected in regions with relatively low system strength levels. The West Murray Zone (WMZ) is one such region, located in the northwest of Victoria, which is far away from synchronous generators and has abundant solar and wind resources. A map of the WMZ is shown in Figure 1(a). Between 2018 and 2023, two IBR-driven sub-synchronous oscillation incidents have been observed by AEMO in the WMZ region. The first incident in 2018 involved an 8 Hz voltage oscillation mode caused by five solar farms in this area; it was triggered by the disconnection of a nearby 220 kV transmission circuit. AEMO identified the source of the 8 Hz oscillations via EMT time-domain simulations [2], and further eliminated the oscillations through controller retuning by working directly with the inverter original equipment manufacturer (OEM) [3]. Another sub-synchronous oscillation incident was observed in 2020 with voltage oscillations at a frequency of 17 Hz [4]. Figure 1(b) shows recorded RMS voltage waveforms at several critical buses in the WMZ during one occurrence of the 17 Hz oscillations.

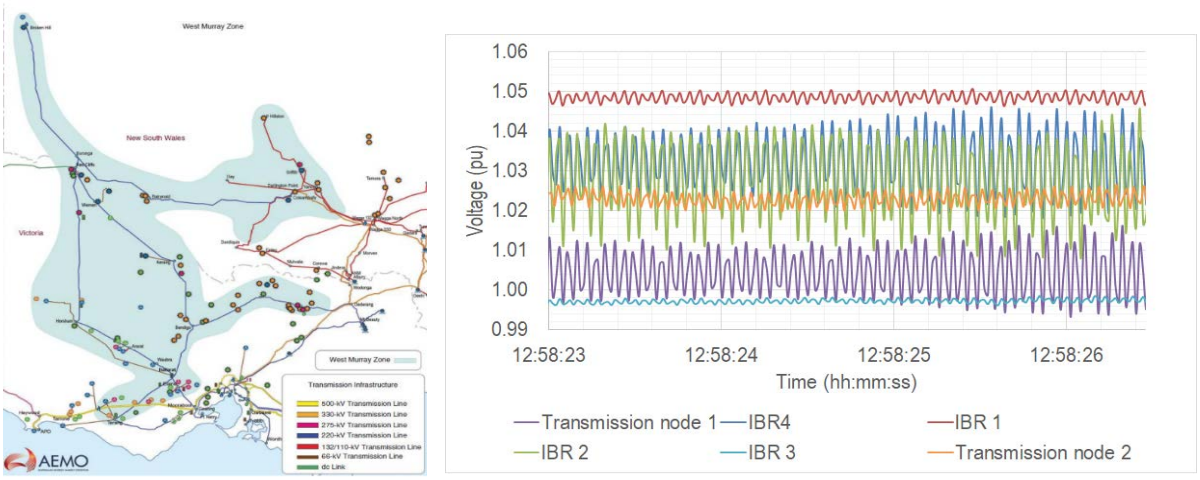

(a) (b)

Figure 1: West Murray Zone (WMZ) . (a) Map of the WMZ , (b) RMS voltages at certain critical buses in the WMZ during a 17 Hz oscillation incident.

These observed oscillation incidents fall under the category of IBR small-signal stability. Many system operators including AEMO increasingly rely on EMT time-domain simulation to replicate such incidents. However, it is not always possible to find out the source of oscillations through EMT time-domain simulations alone. Sometimes control modes and parameter changes performed in the model to replicate an oscillation incident can result false identification of the source of oscillations. It is also difficult to identify the stability margin, or distance to instability, from time-domain simulation results. Other small-signal analysis methods based on white-box modelling, such as eigenvalue analysis, may not be practical, as it could be challenging for system operators to obtain the necessary IBR control block diagrams and configuration parameters due to confidentiality issues. Frequency-domain impedance-based analysis has advantages in addressing these challenges. It relies on the IBR impedance response obtained from black-

box IBR EMT models provided by the generators. It is a top-down approach that does not rely on having knowledge of the underlying IBR control structure details.

This paper presents the methodology and results of an impedance-based analysis [5] of a real-world sub-synchronous oscillation using a frequency domain impedance scan tool developed by the National Renewable Energy Laboratory (NREL) [6].

2. Methodology and Tools

2.1 Impedance-Based Stability Analysis

Standard Approach

The standard approach for the impedance-based stability analysis uses the impedance response of an IBR, say $Z_i(s)$, and that of the grid at the IBR terminal, say $Z_g(s)$, to evaluate whether the connection of the IBR to the grid will create any resonance mode(s) with insufficient or negative damping [7]. It has been used to analyse many different IBR small signal stability problems [8] [9] [10]. Figure 2 illustrates how the small-signal dynamics of a grid-connected IBR can be described by a negative feedback loop based on a Norton equivalent of the IBR with internal impedance $Z_i(s)$ and a Thevenin equivalent of the grid with impedance $Z_g(s)$. The loop gain $L(s)$ of the negative feedback loop is given by:

$$L(s) = \frac{Z_g(s)}{Z_i(s)} \tag{1}$$

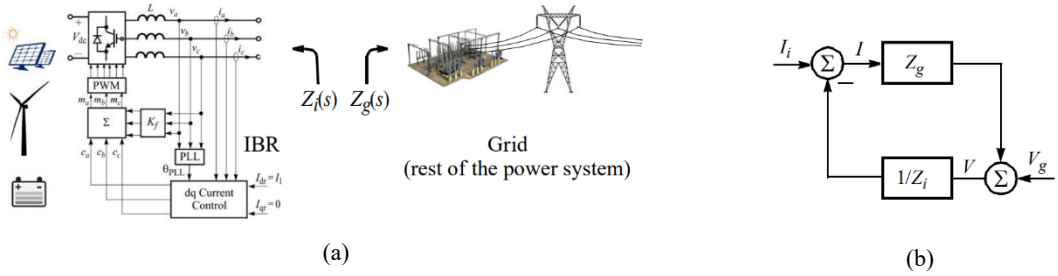

Figure 2: Impedance-based stability analysis of a grid-connected IBR. (a) partitioning of an IBR-grid system, (b) feedback loop representation of small-signal dynamics of an IBR-grid system.

The standard approach for the impedance-based stability analysis method assumes that the grid is stable without the IBR (i.e., when $Z_i(s) = \infty$) and that the IBR is stable if it is connected to an ideal grid with zero internal impedance (i.e., when $Z_g(s) = 0$). If these two assumptions are satisfied, the stability of an IBR – grid system can be determined by checking clockwise encirclements of the critical point (-1, 0) on the complex s-plane using the Nyquist plot of loop gain $L(s)$.

Limitations of the Standard Approach

While the standard form of the impedance-based analysis is effective for a single IBR system, it faces scalability issues when applied to a large power system with multiple IBRs connected. The stability of such a power system can be analyzed using the standard form of the impedance-based stability analysis method by applying the generalized Nyquist criteria to the following loop gain [11]:

$$\boldsymbol{L(s) = Z_g(s) \cdot Y_i(s)} \tag{2}$$

where $\boldsymbol{Z_g(s)}$ is a transfer matrix representing the impedance of the transmission network looking from the POIs of all the IBRs, and $\boldsymbol{Y_i(s)}$ represents a diagonal transfer matrix with admittances of all the IBRs as its diagonal elements. Both the transmission grid impedance and the IBR impedance are necessary to form the loop gain, and the application of the generalized Nyquist Criteria. It is important as the stability analysis using only the device impedance have to assume a specific form for the network impedance – for example,

the network impedance is commonly represented by an R-L branch with R and L values to represent a specific short-circuit ratio and X/R ratio. This approach cannot identify control interactions of a device with other devices (such as IBRs) in the network.

If there are n IBRs in the network, both $\boldsymbol{Z_g(s)}$ and $\boldsymbol{Y_i(s)}$ are at minimum n^{th} order transfer matrices. Moreover, if frequency coupling between the positive- and negative-sequence dynamics is considered [12], which is generally quite significant at frequencies below 100 Hz and cannot be ignored for the analysis of oscillations at low frequencies below 100 Hz, the order of $\boldsymbol{Z_g(s)}$ and $\boldsymbol{Y_i(s)}$ would be $2n$. Hence, significant effort would be required to obtain the impedances of (i) all IBRs involved in the system, including those which are of no interest to system operators, and (ii) that of the network looking from the POIs of all IBRs in the system [11]. The standard approach does not provide flexibility to focus on only a few specific IBRs during stability analysis.

In addition to the above limitation of the standard approach, it is difficult to obtain the network admittance matrix $\boldsymbol{Y_i(s)}$ for a large, real-world power system. Measurement of $\boldsymbol{Y_i(s)}$ requires numerous perturbation experiments involving the injection of perturbation from different POIs and measurement of responses at all the POIs. Such frequency scans are cumbersome and impractical for large power systems for which running even a few seconds of EMT simulations can take a significant amount of time.

Reversed Approach

A reversed approach has been proposed to circumvent the above limitations of the standard approach for stability analysis of large power systems with numerous IBRs [11]. The reversed approach focuses on determining how one selected IBR contributes to the stability or instability of the power system, including contribution to control system interaction with other facilities. Because the reversed approach looks at only one IBR at a time, it requires the impedance/admittance response of only the selected IBR and the rest of the network (including other IBRs) as seen from the POI of the selected IBR. This process can be repeated at any number of IBRs to evaluate how each of them impact the stability of the power system, therefore it greatly simplifies the impedance scan process for a large power system. In addition, the reversed approach allows one to scan the impedance of a device (IBR) and network at its terminal without breaking the network. This is quite important as separate scanning of the IBR and the network as required by the regular approach requires breaking of the network, which is quite difficult to achieve as each IBR in the network must be replaced by an ideal voltage or current source so that to maintain the power flow condition before proceeding with the network scan. Because network might contain more complex equipment such as STATCOM, synchronous condensers, etc., the network-breaking method is not feasible for large real world power systems. The reversed approach avoids these problems by enabling network scan directly in the integrated EMT model breaking the model at IBR connection points.

The reversed approach can be summarized as follows: if a power system is stable when an IBR is connected to it, then the stability of the power system when the IBR is disconnected can be determined by checking for counterclockwise encirclements of the critical point by the Nyquist plot of loop gain $L(s)$. The power system remains stable when the IBR is disconnected if the Nyquist plot does not encircle the critical point, and the power system will become unstable if the Nyquist plot encircles the critical point in the counterclockwise direction. The change in frequency and damping of a resonance mode of a power system when an IBR is disconnected can be determined from the nodal impedance response at the POI of the IBR under both connected and disconnected status of the IBR. The nodal impedance at the POI of an IBR, such as the one shown in Figure 2(a), is defined as follows:

$$Z_n(s) = \begin{cases} Z_g(s) & \text{without IBR} \\ \frac{Z_g(s) \cdot Z_i(s)}{Z_g(s) + Z_i(s)} & \text{with IBR} \end{cases} \tag{3}$$

Note that the loop gain $L(s)$ and impedances $Z_g(s)$, $Z_i(s)$, and $Z_n(s)$ are all second-order transfer matrices as frequency coupling between the positive- and negative-sequence dynamics is considered for the analysis of

subsynchronous oscillations; however, non-bold letters are used in notations in the rest of the paper for the sake of simplicity.

2.2 Steps for Impedance-Based Analysis of Oscillations in Wide-area System

Both the standard and reversed approaches need to be applied for the impedance-based stability analysis of a wide-area power system using the following steps at each IBR of interest:

- **Step 1, SMIB IBR Scan:** The impedance response of a selected IBR, $Z_i(s)$, is obtained by connecting it to an infinite bus, and is used to evaluate whether the IBR has any internal resonance modes with low damping and if the IBR becomes unstable when connected to an inductive grid with a particular short circuit ratio (SCR) and X/R ratio. The analysis is performed at a few operating points that cover the typical operational envelope of the IBR. This step uses the standard approach for the impedance-based stability analysis.
- **Step 2, Wide Area Network Scan**: The impedance response of the grid at the terminal of the selected IBR, $Z_g(s)$, is obtained using the wide area network model including other IBRs. The grid impedance response is obtained for different operating and dispatch conditions of IBRs in proximity. Each grid impedance response is used to evaluate the impact of the removal of the selected IBR on the frequency and damping of the oscillation modes in the system. The selection of scan conditions is done iteratively to evaluate how they influence control interactions among IBRs. The grid impedance scans, $Z_g(s)$, obtained in this step are used in conjunction with the IBR impedance scans, $Z_i(s)$, obtained in the first step. This step uses both the standard and reversed approaches for the impedance-based stability analysis.

The above steps are performed successively at different IBRs of interest to evaluate how each of them impact the frequency and damping of the oscillation modes in the WMZ in the frequency range where oscillations have been observed in the field.

2.3 Impedance Scan Process

The impedance-based stability analysis process described in this paper focuses on one IBR at a time for evaluating its impact on the stability of a power system. This approach requires the impedance response of the IBR being analyzed, and the grid impedance seen at the terminal of the IBR which also includes other IBRs in the system. NREL has developed software to simultaneously scan the impedance response of an IBR, as well as the grid at its terminal using EMT simulations. The details of the software can be found in [13]. In practice, an impedance scan block is inserted between an IBR and the rest of the grid in a compatible EMT simulation environment. This block successively injects voltage perturbations of different frequencies in series between the IBR and the rest of the grid and records the three-phase voltages and currents on both sides for further processing. The frequency range, resolution, and magnitudes of the perturbation voltage signals are adjustable by the impedance scan software. The recorded data are then postprocessed by the software, to derive and plot impedance/admittance responses of the IBR and the grid. The stability analysis at IBR can then be conducted using the scanned IBR impedance response in conjunction with either the scanned impedance response of the grid (wide area network analysis), or a grid strength condition specified in terms of SCR and X/R ratio (SMIB analysis).

3. Study Scenarios

Based on field measurements of the voltage oscillation data recorded by PMUs in the WMZ, the oscillation likely involved five solar farms due to the area in which it manifested, and the largest voltage oscillation magnitudes have been observed near the connection points of three solar farms in the region [4]. Therefore, the impedance analysis has focused on these three solar farms. In the first step, impedance scans were

performed separately at the three solar farms connected in a SMIB configuration. The stability of each solar farm was determined using their impedance response for different SCR and X/R ratio of a hypothetical inductive grid at their terminals. In the second step, impedance scans were performed at the three solar farms connected in the wide area network model. The stability of the wide-area system was determined in this step for different operating and dispatch conditions at the three solar farms, to determine each of their impact to the system stability. The impedance scans considered different permutations of the following potential contributing factors: solar farm active power output, solar farm reactive power output, solar irradiance levels, solar farm dispatch status (wide area network scan only), and network outage conditions (wide area network scan only).

The impedance measurement process is automated, and the measured impedance can be reused for the stability analysis with the impedance measurement from the SMIB scans. The impedance measurement for an IBR in a SMIB configuration would take 2 – 4 hours for one operating condition, depending on the frequency range and resolution, while it could take 2 – 4 days to complete an impedance measurement in a wide-area network model for one operating condition. There are several reasons for exceedingly long scan time as described in the following: (1) The size and complexity of the wide-area network model including all the IBR models implied that EMT simulations run at much slower speeds compared to EMT simulations of a single IBR in SMIB configuration. (2) The wide-area model needs to run till steady state for each frequency point in the frequency scan before voltage perturbations are injected for obtaining the network impedance.

4. SMIB Analysis at Solar Farms

4.1 Solar Farm 1

Figure 3 shows the sequence admittance response of Solar Farm 1 (SF-1) for high and low irradiance conditions obtained by connecting the farm in a SMIB configuration. It can be seen from Figure 3(b) that for the low irradiance condition, the solar farm exhibits an underdamped resonance near 17 Hz in $Y_{nn}(s)$ element of the sequence admittance. It is possible that this underdamped resonance is responsible for the 17 Hz oscillations in the wide-area system.

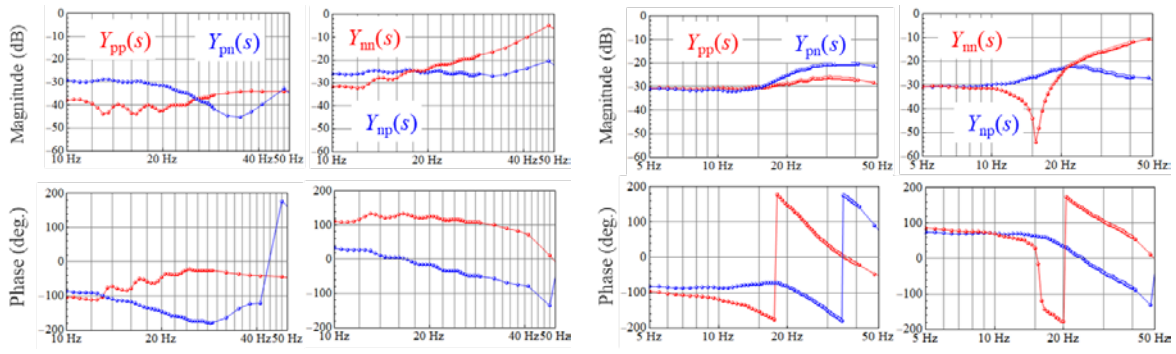

(a) (b)

Figure 3: Sequence admittance response of SF-1 for (a) high irrandiance and (b) low irradiance conditions.

Figure 4 shows results of the impedance-based stability analysis of SF-1 under the low irradiance condition using the impedance response shown in Figure 3(b) for two different grid conditions. The nodal impedance response of $Z_n(s)$ and the Nyquist plot of loop gain $L(s)$ in Figure 4(a) indicate that SF-1 would be unstable at around 17 Hz when the grid SCR is 2.1. This is evident from the clockwise encirclement of the critical point by the Nyquist plot with the frequency at encirclement being around 17 Hz.

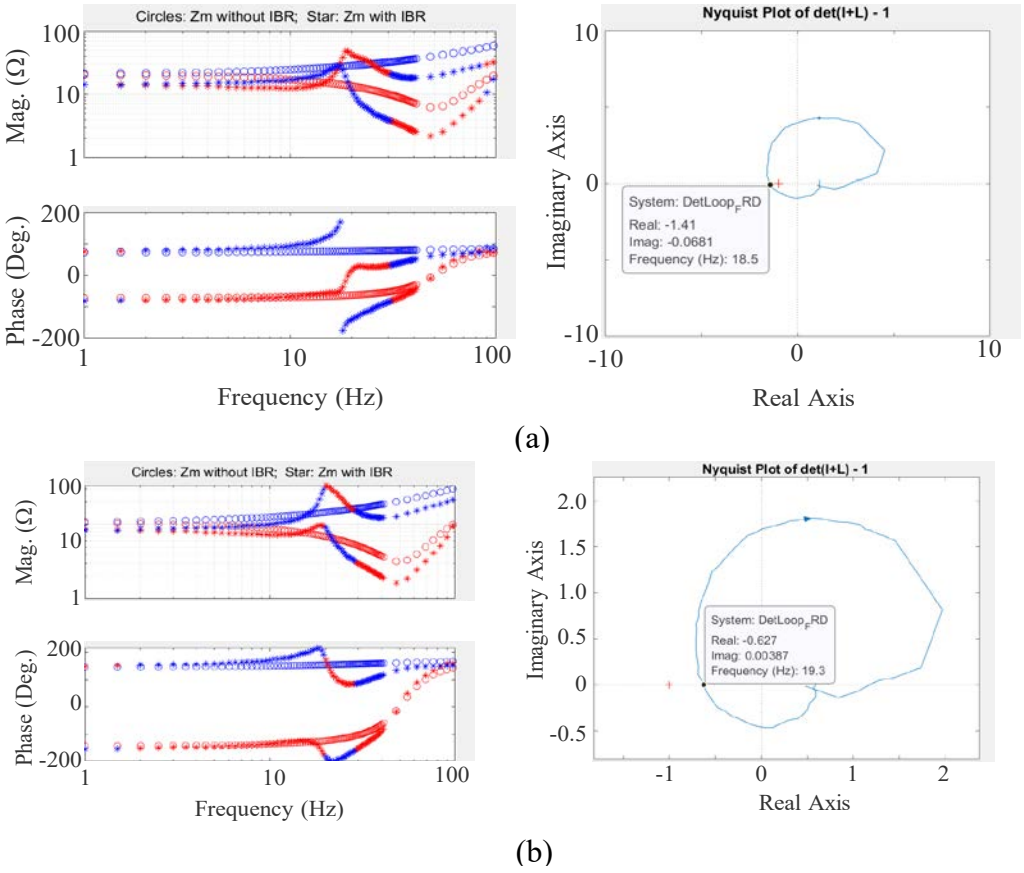

Figure 4: Stability analysis of SF-1 under a low irradiance condition in a SMIB configuration for two different grid strength conditions. (a) SCR = 2.1, X/R = 3.2; (b) SCR = 4.1, X/R = 3.2.

Figure 4(b) shows stability analysis using the same impedance scan of SF-1 from Figure 3(b) for grid SCR of 4.1, indicating that the solar farm is stable for a grid SCR of 4.1. It is important to note that similar analysis can be performed by NREL's impedance scan software for any grid SCR and X/R ratio in just a few seconds without repeating the impedance scan of the solar farm to identify its stability boundary in terms of the SCR of the grid at the POI. Time domain simulations also confirmed the findings from the impedance-based stability analysis.

4.2 Solar Farm 2

Figure 5(a) shows the admittance scan response of Solar Farm 2 (SF-2) for a low irradiance condition obtained in a SMIB configuration. It shows an underdamped resonance at 17 Hz like SF-1 for the low irradiance condition. Figure 5(b) and (c) shows stability analysis results of the solar farm for the low irradiance condition for grid SCR of 2.1 – they predict instability at around 17 Hz.

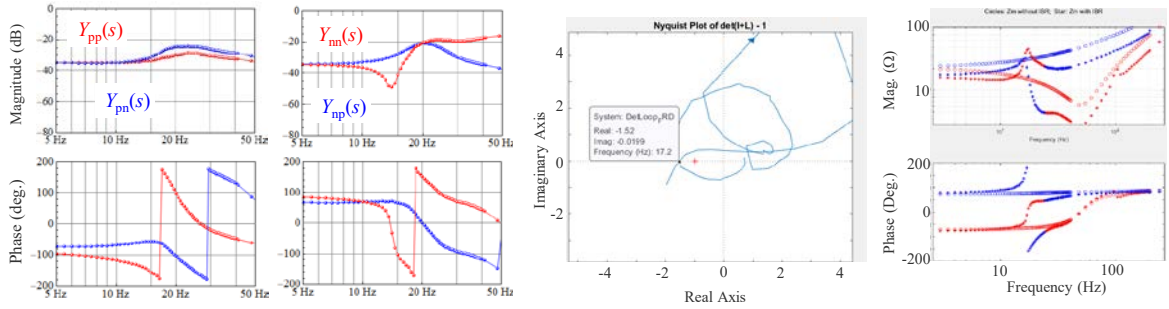

Figure 5: Stability analysis at SF-2 in a SMIB configuration under a low irradiance condition. (a) sequence admittance response of the SF-2, (b) Nyquist plot of loop gain $L(s)$ and (c) response of the nodal impedance at the POI of the SF-2 with (plot with asterisks) and without (plot with circles) the solar farm. Inductive grid with SCR of 2.1 and X/R ratio of 3.2 is used for the stability analysis.

4.3 Solar Farm 3

The impedance scans of Solar Farm 3 (SF-3) for different irradiance conditions (not included here due to space constraints) reveal an underdamped resonance mode at 17 Hz during a low irradiance condition. The mode becomes unstable when the grid SCR is around 2.1. This is similar behavior to SF-1 and SF-2. Both SF-2 and SF-3 can operate stably at high SCR conditions, like SF-1.

4.4 Outcome of SMIB Impedance Assessment

Impedance-based stability analysis at the three solar farms in a SMIB configuration revealed an underdamped mode in each of the three farms at 17 Hz for a low irradiance operating condition. It showed that this mode becomes unstable whenever any of the three farms are connected to a weak grid with an SCR at POI of around 2.1. However, these findings alone do not provide sufficient clarification regarding which farm has the largest contribution to the root cause of the 17 Hz oscillations, when they are all connected to the wide area power system. In addition, the impedance-based stability analysis in a SMIB configuration modelled the grid using an ideal voltage source connected in series with an R-L branch. However, the grid impedance seen at the connection point of an IBR can be "modified" by nearby IBRs, so that the actual grid impedance seen by the IBR may not be reasonably presented by the impedance of an R-L branch. The next section will further discuss the impact on the grid impedance of nearby IBRs, and the findings of the impedance-based analysis of the wide-area system, when all the solar farms are connected to the wide area power system.

5. Wide Area Network Scan at Solar Farms Connection Points

In the wide area network scan study, impedance scans are performed using an EMT model of the wide area network at a selected solar farm to obtain the impedance/admittance response of both the grid seen by the selected solar farm as well as that of the solar farm. We have first focused on SF-2 in the wide area network scan study because it has the lowest SCR at its POI among the three solar farms. First, the grid seen at the POI of SF-2 is scanned using an operating condition at SF-2 that results in stable operation of the wide area system EMT model – this is necessary as the network scan cannot be performed if the wide area system EMT model is unstable. In the next step, the scanned grid impedance seen from SF-2 can be used for impedance-based stability analysis in conjunction with the scanned impedance response of SF-2, obtained either during the wide area network scan or during previous SMIB configuration scans. This process is repeated at SF-1 and SF-3 for different operating and dispatch conditions at the three solar farms.

5.1 Solar Farm 2

Base Case

Figure 6(a) shows the sequence admittance response of the grid seen from the POI of SF-2. This admittance response is obtained when the irradiance at Solar Farm 1 and 3 are kept at a high level. Figure 6(b) shows the Nyquist plot of the loop gain, $L(s)$, using the admittance response of the grid seen from SF-2 from Figure 6(a), and the admittance response of SF-2 with a low irradiance condition from Figure 5(a). Although the Nyquist plot does not encircle the critical point, it is close to an encirclement in the clockwise direction and crosses the real axis at 17 Hz – this indicates that SF-2 forms a resonance mode with the grid at around 17 Hz. The same interpretation can be obtained from Figure 6(c), which shows the response of the nodal impedance, $Z_n(s)$, at the POI of SF-2 with the solar farm (plot with asterisks) and without the solar farm (plot with circles). Because the Nyquist plot does not encircle the critical point, it is interpreted that the resonance mode at 17 Hz has positive damping.

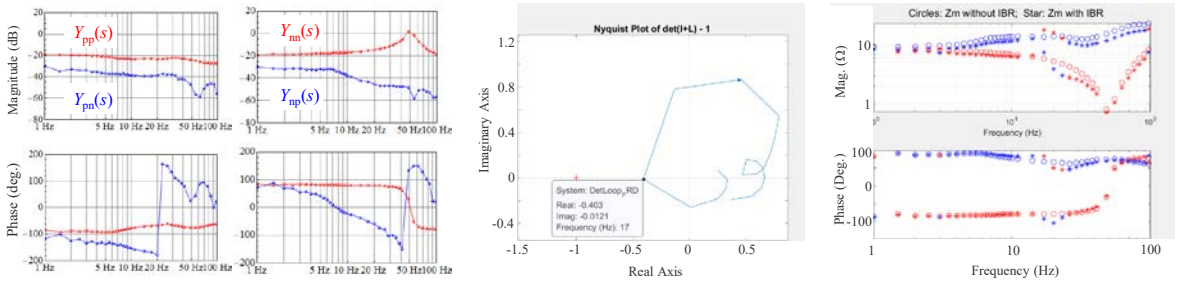

(a) (b) (c)

Figure 6: Stability analysis at SF-2 under a low irradiance condition using a wide area network scan obtained when SF-1 and SF-3 were set up for a high irradiance condition. (a) sequence admittance response of the network seen from SF-2, (b) Nyquist plot of loop gain $L(s)$, and (c) nodal impedance with (asterisks) and without (circles) SF-2 connected to the grid.

Stressed Case

Figure 7 shows results from a wide area network scan study similar to the base case at SF-2 but with a low irradiance level at SF-1 and SF-3. This excites the 17 Hz mode of SF-1 and SF-3 in addition to that of SF-2. As can be seen from Figure 7(a) that the grid seen from SF-2 now contains a resonance mode at 23 Hz during a low irradiance condition at SF-1 and SF-3. The Nyquist plot in Figure 7 marginally encircles the critical point in a clockwise direction with the frequency at encirclement being 17.2 Hz. This indicates instability or negative damping at around 17 Hz. The nodal impedance response in Figure 7(c) shows that the grid has a damped resonance mode at around 23 Hz in the absence of SF-2 (see plot with circles); the response with SF-2 (plot with asterisks) shows that the connection of SF-2 moves the 23 Hz mode to 17 Hz and reduces its damping to a low negative value.

The above analysis shows that SF-2 creates a poorly damped mode at 17 Hz for a low irradiance condition in the base case of the grid, and the same mode becomes unstable in the stressed case of the grid when SF-1 and SF-3 also have low irradiance levels. Figure 8 shows active and reactive power output as well as the voltage at the POI of the three solar farms for the stressed grid condition (low irradiance level at SF-1, SF-2, and SF-3). It also shows that the system initially operates stably without any oscillations; however, the oscillations occur when the irradiance level at SF-2 is reduced to a low level at t = 16s in the simulation. This confirms the outcome of impedance-based stability analysis results presented in Figure 7.

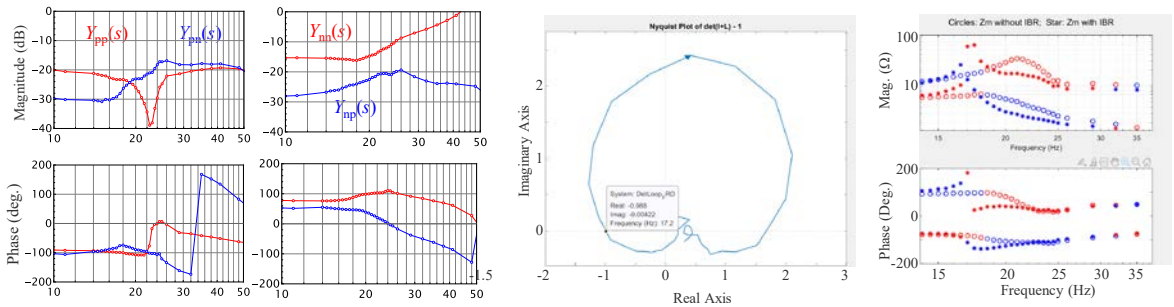

Figure 7: Stability analysis at SF-2 under a low irradiance condition using a wide area network scan obtained when SF-1 and SF-3 models were set up for a low irradiance condition. (a) sequence admittance response of the network seen from SF-2, (b) Nyquist plot of loop gain $L(s)$, and (c) nodal impedance with (asterisks) and without (circles) SF-2.

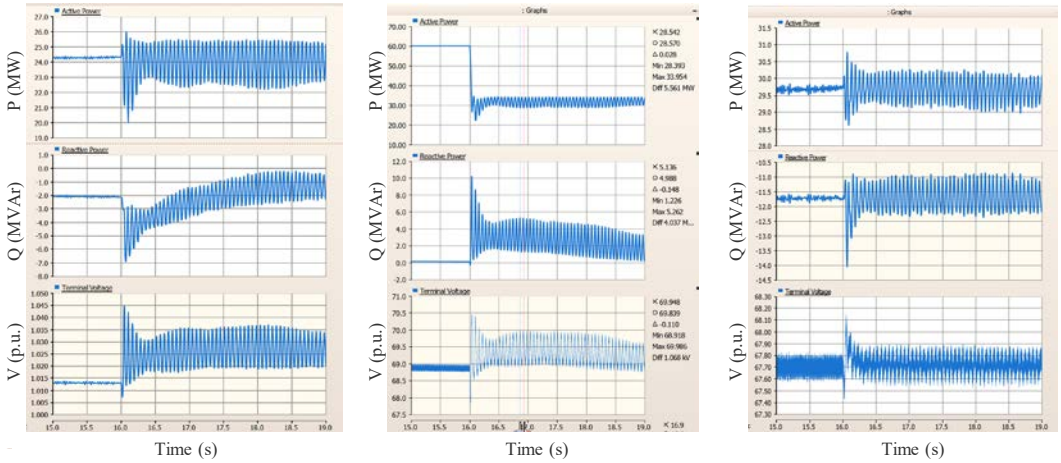

Figure 8: EMT simulation response of the wide-area system showing unstable oscillations when irradiance at SF-2 is changed from a high to a low value. The irradiance at SF-1 and SF-3 was kept unchanged at a low value. (Left) SF-1 time domain P,Q,V response, (Middle) SF-2 time domain P,Q,V response, (Right) SF-3 time domain P,Q,V response.

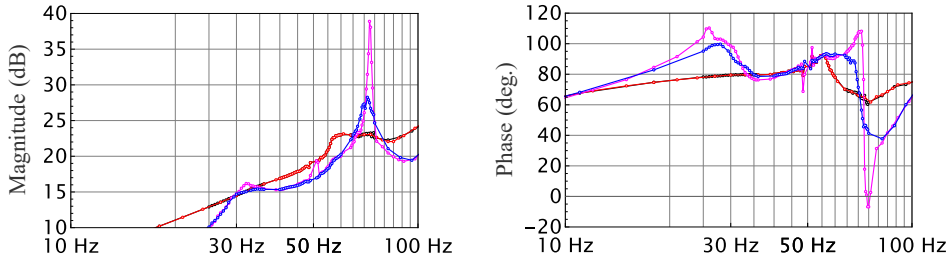

Figure 9: Positive sequence impedance response of the network as seen from SF-2 for different dispatch/operating conditions of SF-1 and SF-3. Black Lines : SF-1 and SF-3 are disabled; Red Lines : SF-1 and SF-3 have high irrandiance; Blue Lines : SF-1 has low irradiance and SF-3 is disabled; Pink Lines : SF-1 and SF-3 have low irradiance.

In addition to the two cases presented above, the impedance/admittance response of the grid seen from SF-2 was scanned for several different operating/dispatch conditions at SF-1, SF-3, and other IBRs in the grid. Figure 9 summarizes some of these scans – it shows the positive-sequence impedance response of the grid

seen from SF-2 for different scan conditions. The black lines show the response when SF-1 and SF-3 are not connected. It does not show any underdamped resonance in the grid. The red lines show the grid impedance response when SF-1 and SF-3 are connected with a high irradiance level; the response is indistinguishable from the black lines, indicating that SF-1 and SF-3 do not create any new resonance modes in the system when they have a high irradiance level. The blue lines show the grid impedance response when SF-1 has a low irradiance level and SF-3 is not connected; it shows an underdamped mode at 73 Hz in the positive-sequence impedance response; this is equivalent to a 23 Hz mode in phasor variables such as power output, voltage magnitude, frequency, etc. The pink lines show the response when SF-1 and SF-3 are both connected at a low irradiance level; it shows that the damping of the 73 Hz resonance (again, equivalent to a 23 Hz mode in the phasor domain) is even lower than the previous case.

The above analysis shows that low irradiance levels at SF-1 and SF-3 stresses the grid by creating an underdamped mode at 23 Hz. From the grid impedance response in Figure 9, the resonance mode created by SF-1 and SF-3 with a low irradiance condition can be interpreted as significant increase in the grid impedance at the resonance frequency compared to the base case (with SF-1 and SF-3 at a high irradiance level) and hence as a reduction in grid strength at the resonance frequency. As shown in Figure 7, the 23 Hz mode is pushed to instability by SF-2 when it has a low irradiance level, and it also moves the frequency of the mode to 17 Hz. The wide area impedance scan study also found that the dispatch of SF-2 at a low irradiance level is a necessary condition for instability to exist in the grid at 17 Hz; the dispatch of either SF-1 or SF-3 at a low irradiance level further deteriorates the stability margin, but removal of either of SF-1 or SF-3 will not eliminate the possibility of 17 Hz oscillations in the grid.

5.2 Solar Farm - 1

Once it was confirmed from the wide area network scan study at SF-2 that the dispatch of SF-2 at a low irradiance level is the primary source of instability at 17 Hz in the grid, the focus was moved to studying SF-1 and SF-3 without dispatching SF-2 in the grid to verify the primary contributor to the 23 Hz mode in the grid. Figure 10 shows one of several results of stability analysis done for conditions when SF-2 was not connected from the grid. The figure shows stability analysis at SF-1 when both SF-1 and SF-3 are connected with a low irradiance level. Figure 10(a) shows nodal impedance response at the POI of SF-1 when SF-1 is connected (plot with asterisks) and when SF-1 is disconnected (plot with circles). It can be interpreted from the response that SF-1 is the primary contributor to the creation of the 23 Hz mode in the grid, as the mode is absent when SF-1 is not connected. A similar interpretation can be made from the Nyquist plot of loop $L(s)$ at SF-1 shown in Figure 10(b). Hence, SF-1 is found to be the second significant contributor to oscillations in the grid after SF-2. Mitigation of the internal 17 Hz mode of SF-2 in the present grid condition will significantly reduce the risk of oscillations.

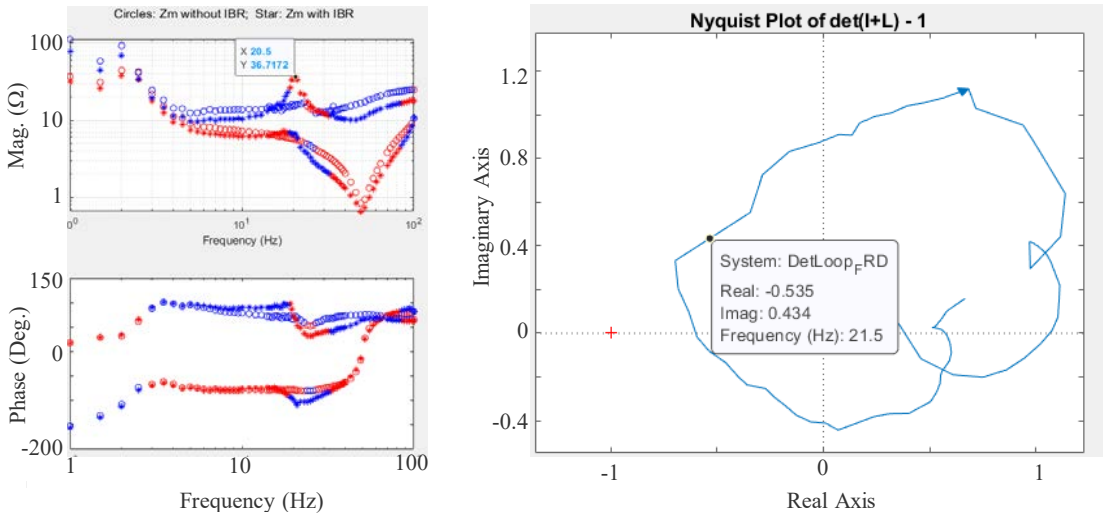

Figure 10: Stability analysis at SF-1 under a low irradiance condition using a wide area network scan obtained when SF-2 is not connected and SF-3 is connected at a low irradiance level. (a) Nodal impedance response at the POI of SF-1 with (asterisks) and without (circles) SF-1 connected to the grid, and (b) Nyquist plot of loop gain $L(s)$.

5.3 Summary of Wide-area Impedance Assessment

The internal 17 Hz modes were first found in all three solar farms during the SMIB analysis. The wide-area network scan study showed that under certain dispatch conditions, the 17 Hz modes in the solar farms interact with each other and result in a poorly damped system-wide 17 Hz oscillations. In particular, the dispatch of SF-2 at a low irradiance level is found to be the key condition that results in instability and oscillations at 17 Hz in the wide-area network. The operation of SF-1 and SF-3 at low irradiance levels increases both the stress on the grid and the risk of oscillations at 17 Hz. The contribution to instability of SF-1 is found to be higher than that of SF-3. Hence, the mitigation strategy for 17 Hz oscillations in the grid should prioritize control updates at SF-2 with a focus on eliminating the internal 17 Hz mode in the solar farm.

The results of the wide-area impedance assessment are summarized in the following table.

Table 1: Summary of wide-area impedance-based analysis

Case	Is solar farm connected (Y/N)			Solar farm irradiance level (High/Low)			Resonance mode in grid seen by SF-2	Resonance mode in SF-2	Overall system resonance mode	Risk of 17Hz oscillations
	SF-1	SF-2	SF-3	SF-1	SF-2	SF-3				
1	Yes	Yes	Yes	High	Low	High	None	17Hz	17Hz	Low
2	No	Yes	No	N/A	Low	N/A	None	17Hz	17Hz	Low
3	Yes	Yes	Yes	Low	Low	Low	23Hz	17Hz	17Hz	High
4	Yes	Yes	No	Low	Low	N/A	23Hz	17Hz	17Hz	High
5	Yes	No	Yes	Low	N/A	Low	23Hz	N/A	23Hz	None
6	Yes	No	No	Low	N/A	N/A	23Hz	N/A	23Hz	None

6. Conclusion

The impedance scan study of the WMZ in the NEM power system has provided several insights regarding the root cause of 17 Hz oscillations observed in the field. The impedance scan study has shown that such analysis is not only able to identify the largest contributors to oscillations or instabilities in power systems with a high penetration level of IBRs, but can also confirm the mechanism by which each IBR is contributing either positively or negatively to the stable operation of a power system. Impedance-based analysis can support small-signal stability analysis by using vendor-supplied blackbox EMT models of IBRs which were already available to the system operator, thereby eliminating IP issues that may arise if requiring linearized open-box models from OEMs.

The impedance scan study found an internal 17 Hz mode in three solar farms in the wide-area power system; this mode becomes unstable for certain operation/dispatch conditions of the three solar farms, resulting in the 17 Hz oscillations observed in the field. Specifically, the dispatch of one particular solar farm at a low irradiance level was identified as a necessary condition for the 17 Hz oscillations. It was also found that the dispatch of the other two solar farms at a low irradiance level can further reduce the damping of the 17 Hz oscillations. However, removal of either of these solar farms will not eliminate the risk of these oscillations.

It was found from the wide-area impedance-based analysis that certain IBRs can increase the effective grid impedance at non-fundamental frequencies at the POI of other IBRs. Such a reduction in grid strength at non-fundamental frequencies can increase the risk of unstable or poorly damped oscillations. This highlights the limitation of metrics such as the SCR in quantifying grid strength, as such metrics focus only on power system behaviour at the fundamental frequency. Impedance response over a broad frequency range can more effectively estimate grid strength for power systems with a high IBR penetration level. Future work will evaluate the effectiveness of control updates at solar farms in mitigating oscillations in the WMZ, and will use the impedance-based analysis for evaluating the effectiveness of grid-forming resources and synchronous condensers in improving stability of the WMZ as more IBRs are integrated in the area.

Acknowledgement

This work was authored in part by Alliance for Sustainable Energy, LLC, the manager and operator of the National Renewable Energy Laboratory for the U.S. Department of Energy (DOE) under Contract No. DE-AC36-08GO28308. Funding provided by U.S. Department of Energy Office of Energy Efficiency and Renewable Energy Wind Energy Technologies Office.

BIBLIOGRAPHY

[1] AEMO, Quarterly Energy Dynamics Q3, 2023, available online at: https://aemo.com.au/-/media/files/major-publications/qed/2023/qed-q3-2023-report.pdf?la=en&hash=165E68BF9A6DAF100B56CFAAC437CE20

[2] B. Badrzadeh, N. Modi, N. Crooks, and A. Jalali, "Power system operation with reduced system strength for inverter-connected generation during prior outage conditions." *CIGRE Science and Engineering Journal* 17 (2020): 141-149.

[3] A. Jalali, B. Badrzadeh, J. Lu, N. Modi, and M. Gordon (2021), "System strength challenges and solutions developed for a remote area of Australian power system with high penetration of inverter-based resources," *CIGRE Science and Engineering Journal*, 27-37.

[4] AEMO, West Murray Zone Sub-synchronous oscillation, October 2022, available online at: https://aemo.com.au/-/media/files/electricity/nem/network_connections/west-murray/high-level-summary-of-wmz-subsynchronous-oscillations.pdf?la=en

[5] S. Shah, P. Koralewicz, V. Gevorgian, H. Liu, and J. Fu, "Impedance methods for analyzing stability impacts of inverter-based resources: stability analysis tools for modern power systems," *IEEE Electrification Magazine*, vol. 9, no. 1, pp. 53-65, Mar. 2021.

[6] S. Shah, P. Koralewicz, and E. Mendiola, GIST (Grid Impedance Scan Tool) [SWR-22-73]. Computer software. USDOE Office of Energy Efficiency and Renewable Energy (EERE), Renewable Power Office. Wind Energy Technologies Office. 21 Sep. 2022. Web. doi:10.11578/dc.20221214.3.

[7] J. Sun, "Impedance-based stability criterion for grid-connected inverters," *IEEE Transactions on Power Electronics*, vol. 26, no. 11, Nov. 2011.

[8] M. Cespedes and J. Sun, "Impedance Modeling and Analysis of Grid-Connected Voltage-Source Converters," in IEEE Transactions on Power Electronics, vol. 29, no. 3, pp. 1254-1261, March 2014

[9] L. Fan and Z. Miao, "Time-Domain Measurement-Based DQ-Frame Admittance Model Identification for Inverter-Based Resources," in IEEE Transactions on Power Systems, vol. 36, no. 3, pp. 2211-2221, May 2021

[10] L. Zhao, X. Wang and Z. Jin, "Impedance-Based Dynamics Analysis for DC-Link Voltage-Synchronized Voltage-Source Converters," in IEEE Transactions on Power Electronics, vol. 38, no. 9, pp. 10829-10844, Sept. 2023

[11] S. Shah, W. Yan, P. Koralewicz, E. Mendiola, and V. Gevorgian, "A reversed impedance-based stability criterion for IBR grids," in *Proc. 21st Wind and Solar Integration Workshop*, The Hague, Netherlands, Oct. 2022. [Online]: https://www.nrel.gov/docs/fy23osti/84000.pdf

[12] S. Shah and L. Parsa, "Impedance modeling of three-phase voltage source converters in dq, sequence, and phasor domains," *IEEE Transactions Energy Conversion*, vol. 32, no. 3, pp. 1139-1150, Sep. 2017.

[13] "Impedance Measurement." NREL.gov. https://www.nrel.gov/grid/impedance-measurement.html